Thesis for the degree of Licentiate of Engineering

Gyrokinetic simulations of turbulent particle and heat transport in tokamaks

Daniel Tegnered

Department of Earth and Space Sciences
Chalmers University of Technology
Göteborg, Sweden, 2015

Gyrokinetic simulations of turbulent particle and heat transport in tokamaks
Daniel Tegnered

Department of Earth and Space Sciences
Chalmers University of Technology
SE-412 96 Gothenburg
Sweden
Telephone +46 31 772 1000

Cover:
The image shows density fluctuations in a cross section of a flux tube at the low field side of the tokamak at three different time points.

Printed in Sweden by
Chalmers Reproservice
Göteborg, Sweden, 2015

GYROKINETIC SIMULATIONS OF TURBULENT PARTICLE AND HEAT TRANSPORT IN TOKAMAKS

Daniel Tegnered
Department of Earth and Space Sciences
Chalmers University of Technology

Abstract

Fusion power is one of few viable sustainable means of energy production. The tokamak is arguable the most mature technology to magnetically confine fusion plasmas. In these devices, heat and particle transport is dominated by small-scale turbulent fluctuations. Recent advances in high performance computing have made it possible to study these phenomena in detail.

The Joint European Torus (JET) is currently the largest tokamak in operation. Recently, the plasma facing components of JET were changed from carbon to metal — beryllium and tungsten. This in order to better align with the design foreseen for ITER, a next-generation device under construction in Cadarache in France. The change to this so-called ITER-like wall at JET has had several consequences.

Firstly, it introduces new impurities into the plasma. Impurities, any ion that is not a reactant in the fusion reactions, are detrimental to the fusion power as they dilute the plasma and can radiate energy. It is therefore important to study the transport of impurities and how it is affected by different operational parameters, such as the cross-sectional shape of the plasma.

Secondly, the change of wall material has led to a degradation in energy confinement for certain types of discharges at JET. Energy confinement must be optimized in future fusion devices in order for them to be economically viable.

The present thesis aims at an improved understanding of these urgent issues by means of gyrokinetic simulations of particle and heat transport driven by Ion Temperature Gradient (ITG) and Trapped Electron (TE) mode turbulence.

Keywords: fusion, plasma physics, tokamak, turbulence, transport, impurities, gyrokinetics, Joint European Torus, ITG, TEM

List of appended papers

[A] A. Skyman, L. Fazendeiro, D. Tegnered, H. Nordman, J. Anderson, P. Strand. Effects of the equilibrium model on impurity transport in tokamaks. *Nuclear Fusion*, 54(1):013009, 2014.

[B] A. Skyman, D. Tegnered, H. Nordman, P. Strand. Gyrokinetic modelling of stationary electron and impurity profiles in tokamaks. *Physics of Plasmas*, 21(9):092305, 2014.

[C] D. Tegnered, P. Strand, H. Nordman, C. Giroud, Hyun-Tae Kim et al. Comparative gyrokinetic analysis of JET baseline H-mode core plasmas with carbon wall and ITER-like wall. Submitted to the JET Pinboard, 2015.

Other contributions

[D] A. Skyman, J. Anderson, L. Fazendeiro, H. Nordman, D. Tegnered, R. Singh, and P. Strand. Particle transport in ion and electron scale turbulence. In *Proceedings of 24th Fusion Energy Conference* IAEA CN-197, 2012.

[E] A. Skyman, H. Nordman, J. Anderson, L. Fazendeiro, P. Strand, D. Tegnered, and R. Singh. Turbulent particle transport driven by ion and electron modes. In *Proceedings of EPS 2012, Europhysics Conference Abstracts*, 2012.

[F] L. Fazendeiro, A. Skyman, D. Tegnered, H. Nordman, P. Strand, and J. Anderson. Gyrokinetic simulations of turbulent transport in JET-like plasmas. In *Proceedings of EPS 2013, Europhysics Conference Abstracts*, 2013.

[G] D. Tegnered, P. Strand, H. Nordman, L. Fazendeiro, and A. Skyman. Predictive simulations of impurity transport at JET. In *Proceedings of EPS 2013, Europhysics Conference Abstracts*, 2013.

[H] D. Tegnered, A. Skyman, H. Nordman, and P. Strand. Gyrokinetic modelling of stationary electron and impurity profiles in tokamaks. In *Proceedings of EPS 2014, Europhysics Conference Abstracts*, 2014.

Acknowledgements

I would like to express my sincerest gratitude to my supervisor Dr. Pär Strand for his constant support and encouragement. An equally huge thank you to professor Hans Nordman for always being available and providing copious amounts of helpful comments and good advice. Further, I am grateful to Dr. Andreas Skyman for helping me getting started in the world of fusion and gyrokinetics.

Finally, to Maj Stenmark, family and friends, thank you for unwavering moral support, you are all an inspiration to me.

Contents

Chapter 1

Introduction

1.1 Nuclear fusion

Nuclear fusion is the most common energy source in the universe as it is the energy source of the stars. Two light nuclei collide and fuse into a heavier element. Without this process there would be no elements heavier than hydrogen. The mass of these new elements is not simply the mass of the reactants — it turns out that mass has been lost in the form of energy. The fact that mass can be equated with energy is known from Einstein's famous formula $E = mc^2$, where c is the speed of light in vacuum. The energy lost is equal to the binding energy as it has to be supplied in order for the reactants to separate. The larger the binding energy per nucleon, the more stable the element.

As can be seen in figure 1.1 the binding energy per nucleon is the largest for an isotope of iron, ^{56}Fe. Thus, energy is released when either elements lighter than iron are fused together or when elements heavier than iron are split, as is the case in fission power plants. The masses involved in each reaction are much larger than in chemical reactions so the fuel needed per unit of energy is much lower. However, nuclei will repel each other since they are positively charged, so large temperatures are needed in order to overcome this Coulomb repulsion. The energy needed to overcome the repulsion for two hydrogen nuclei is around 0.4 MeV, corresponding to a temperature of $3 \cdot 10^9$ K. Thus nuclear fusion would be almost impossible without quantum tunnelling, which lowers the needed temperature by at least an order of magnitude.

Large temperatures means that the matter will be ionized — it can thus be in the plasma state, since the frequency of ionizing collisions

will be higher than the frequency of the recombining collisions. The important problem in fusion science is how to confine this hot plasma so that the fusion reactions can occur without too much energy escaping the system. In the stars, the plasma is gravitationally confined. The mass is large enough so that the gravitational forces contain the plasma and the proton-proton chain reaction can occur whereby helium-4 is created from protons in multiple steps. The masses and power densities involved are such that this approach is not feasible on earth.[1]

Another method is to bombard a small pellet of hydrogen with lasers that will compress the matter so fast that the inertia will be enough for fusion reactions to occur before the material is scattered. This method is called inertial confinement fusion. There have been high profile experiments in this area, first and foremost the National Ignition Facility, but the results are thus far disappointing [2].

A third way to confine the plasma is to use the fact that the particles of the plasma, the ions and electrons, are charged and will be subject to the Lorentz force, $\mathbf{F} = q\mathbf{v} \times \mathbf{B}$, where $\mathbf{F}$ is the force on a particle, q is the charge of the particle and $\mathbf{B}$ is the magnetic field. In absence of collisions, they will follow and circle around the magnetic field lines. This method to confine the plasma is called magnetic confinement. The magnetic confinement will be optimized if the topology of the magnetic field is such that the field lines have no endings. One such topology in three dimensions is a torus. Several different schemes to use a toroidally shaped magnetized plasma, that first and foremost differ in the way the magnetic fields are created, have been devised, for example the so called stellerator and the tokamak[2]. The tokamak is considered the most mature technology.

The fusion reaction that is the likeliest to occur, i.e. has the largest cross section at lower temperatures, is not the proton-proton chain of the sun. Instead, it is the reaction between two isotopes of hydrogen, deuterium and tritium. So the reaction foreseen in future fusion power plants is $\mathrm{D} + \mathrm{T} \rightarrow {}^4\mathrm{He} + \mathrm{n} + 17.6\,\mathrm{MeV}$. Five nuclei are involved in the reaction, so 3.5 MeV is released per nucleon. As a comparison, 0.85 MeV is released per nucleon during the fission of U235 and the energy released from burning one molecule of ethanol is just 13.47 eV. The neutron will not be confined by the magnetic field as it is uncharged and will leave

[1] In our Sun the power density of the core is comparable to that of a compost heap [1]

[2] Russian, from toroidal'naya kamera s aksial'nym magnitnym polem (toroidal chamber with an axial magnetic field)[3]

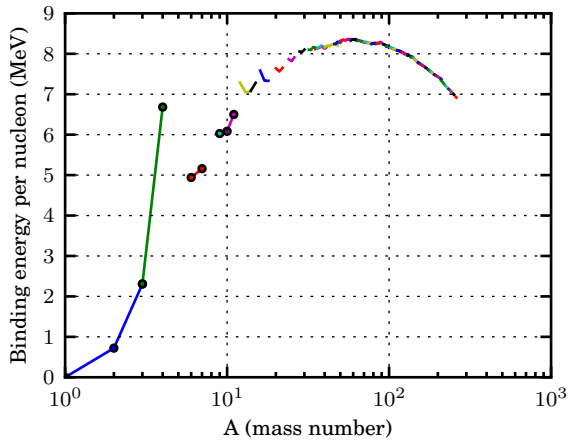

Figure 1.1: Binding energies per nucleon of the most common isotopes, connected isotopes are the same element. The binding energy is the energy that would have to be supplied in order to separate all the nucleons. Data from [4].

the plasma and heat the wall. The charged helium nuclei, the so-called α-particle, on the other hand, will be confined by the magnetic field and serve to heat the rest of the plasma.

1.2 Sustainability

The world energy use in 2012 was around 17 TWy [5]. According to the International Energy Agency's World Energy Outlook 2013 the global energy demand will grow by 30 % by 2035. The UN reference case growth for energy demand until 2030 is 3.6–4.9 TWy, mostly in the lower-middle income part of the world. Meanwhile, the energy efficiency opportunity is just 2.7–3.3 TWy, mostly in the high income part of the world [6]. Given a growing global population and an increase in living standards in the third world, it thus seems unlikely that the world energy demand will decrease in the foreseeable future.

Currently, 82 % of that energy comes from fossil fuels [7]. Fossil fuels are undesirable and unsustainable for a number of reasons, first and foremost in that their release will trigger serious climate change [8]. The finite fossil fuels are also the basis for a multitude of chemical and pharmaceutical products that we must have access to in the future. The list of energy sources that could replace the fossil fuels is however not very

long: renewable sources like wind and solar power, nuclear fission and fusion. Tens of Terawatts worth of production of these energy sources thus needs to be constructed during the coming decades. This might be the single most daunting sustainability challenge that the world currently faces [9].

Renewable energy sources will surely play an important role in the energy mix of the future, but they are not without drawbacks. They can be of limited potential, like hydro power, which prevents them from contributing significantly. Most are very diffuse with a low energy output per unit area. Wind power, for example, have a potential of $2-3\,\mathrm{W/m^2}$ [10], 20 TW of power production would thus require roughly 15 times the area of Sweden. The energy and materials required to construct the energy facilities would also be significant, so a life cycle analysis approach is important. Photovoltaic systems require 11-40 times more copper than fossil generation and wind power demands 6-14 times more iron. In order to build a low-carbon energy system by 2050 two years of copper and one year of iron production is needed [11]. The intermittency of many of the renewable energy sources will also require large investments in so called smart grids and energy storage solutions, this can cost as much as 1 trillion Euros up to 2030 for the European Union alone [12]. Furthermore, even though renewable energy often has a comparable price to fossil based alternatives, it has yet to make a considerable contribution to the energy mix.

Fission power also has its fair share of problems but could be developed to mitigate most of them. In 2005 there was an installed fission power capacity of 369 GW requiring 67 320 tons of uranium annually with estimated total world resources of 4 743 000 tons uranium [13]. With 20 TW of fission power production the resources would thus last only 1.3 years with present technology. At those production levels, the waste would also be a huge problem. Fourth generation breeder reactors could make use of the uranium much more efficiently, reducing the need by a factor 30 or more. The safety aspect, nuclear proliferation and negative public opinion are other obstacles for widespread fission power.

The fact that both renewable energy sources and fission power have failed to make an impact on the energy mix can be due to a number of lock-in mechanisms that act as barriers to diffusion of these technologies. These lock-in mechanisms can be technological in nature. The huge infrastructures that already exists, like petrol stations and natural gas pipe lines, are one such example. They can also be institutional, fossil fuel industries are subsidised to the tune of $200 billion annually [14]. In

order to overcome this techno-institutional lock in, new strong policies are needed from the governments worldwide, but history has shown that the most efficient way of breaking such a techno-institutional complex is with a new transformative technology [14], nuclear fusion could be that technology.

The fuel for future fusion reactors will be deuterium and tritium. Deuterium can be obtained from so-called heavy water through electrolysis. Heavy water is obtained from fresh water through the GS isotopic exchange process [15]. The potential deuterium reserves are vast, 1 part in 6400 in water. Tritium, on the other hand, has a half-life of 12.3 years and is thus not available in nature, but must be produced at the reactor. The intention is to breed the necessary tritium from litium-6 and the neutron from the fusion reaction in a so-called blanket in the reactor wall. The reaction is $^6\mathrm{Li} + \mathrm{n} \rightarrow ^4\mathrm{He} + \mathrm{T} + 4.8\,\mathrm{MeV}$. Consequently, the sources of fuel for a future fusion reactor will be water and lithium, with the latter being the only possible limiting factor. According to the USGS estimates of world resources there are around 40 million tons of lithium available worldwide [16]. The energy content of natural lithium, using the reactions described above, is around 0.86 GWy/ton [17]. Thus, 20 TW of energy production would use 23000 tons of lithium per year and the reserves would last in the order of 2000 years. This can be regarded as a long enough time span for the technology to be seen as sustainable. Furthermore, there are considerable amounts of lithium in sea water (0.17 g per ton) that could potentially be extracted economically in the future [18]. Lithium is, however, just like oil used for a multitude of purposes so using all for energy production is not desirable. If, for example, the global automobile fleet is electrified in the coming decades a considerable amount of lithium will be required for the batteries.

In the reaction above to breed tritium from lithium each fusion reaction only creates one neutron which in the breeding reaction only creates one new triton. Since losses of neutrons are impossible to avoid, so called neutron multipliers will also be needed. Beryllium and lead are two materials that could serve this purpose, and they would be used up in the reactions. It is questionable whether the worldwide resources of beryllium would be enough for a fusion powered world, the situation with lead is much better with the resources lasting in the order of 100 000 years [18].

Other than resources, for nuclear fusion to be called a sustainable energy solution, it should not be a threat to human safety or the environment in general. Nuclear fusion differs greatly from nuclear fission

in that the amount of fuel in the reaction chamber is just in the order of a couple of grams. Furthermore, since the reaction depends on very high temperatures any operational problems would lead to the immediate termination of the reaction. The fuel (lithium and deuterium) is not radioactive, neither is the end product (helium). However, tritium is radioactive and will contaminate materials in the reactor. Furthermore the neutrons from the fusion reactions will activate materials. The choice of materials used to build the reactor is therefore very important, but with the right choice the materials could be recycled in a matter of decades [17]. All in all, fusion reactors would generate activated materials on a scale similar to that of fission power plants but with much lower long term radio toxicity since there would be no spent fuel. Release of tritium in an accident is a concern since tritium could replace hydrogen and can thus contaminate biological systems. However, at most 200 g of tritium released is foreseen as a worst case scenario in the case of an accident [17]. As mentioned, the short half-life also ensures that the area will not be contaminated for long.

Chapter 2

Magnetized fusion plasmas

Plasma is often referred to as the fourth state of matter, besides solid, liquid and gas. On Earth, it is much less common than the other three states of matter. The level of ionization in a gas depends on the temperature and density of the gas. Atoms are ionized when they collide with a particle with high enough energy. At the temperatures we commonly have around us, an atom must have been accelerated to energies much higher than the average by a series of collisions. Consequently, the number of atoms in the gas that have high enough energy goes as e^{-U_i/k_BT} where U_i is the ionization energy of the gas, k_B is the Boltzmann constant and T is the temperature.[1] The ion will stay ionized until it recombines with an electron, the recombination rate will depend on the density of the electrons and go as n_e^{-1}. The degree of ionization for air at room temperature is on the order of $\frac{n_i}{n_e} \approx 10^{-122}$.

But it is not just the level of ionization that determines whether matter is in the plasma state. What makes a plasma different from a gas is the long range Coulomb interactions possible between the charged particles. A useful definition for a plasma is thus [19]

> "A quasi-neutral gas of charged particles which exhibits collective behaviour."

In a gas with neutral particles, these will not interact until they collide, so interaction between more than two particles is uncommon. In contrast, in a plasma the motion of the charged particles will lead to electric currents that create magnetic fields and there will be electric fields caused

[1] In fusion reactors, it is the particles of this tail in the Maxwellian distribution, replenished by scattering collisions, that will undergo fusion reactions.

by temporary concentrations of positive or negative particles. These fields will interact with all the other charged particles — this is the collective behaviour. Quasi-neutrality entails that any concentration of charge will be shielded out in distances that are much smaller than the size of the plasma. This means that the charges will balance out on a macroscopic level and the quasi-neutrality condition, $n_e = \sum_i Z_i n_i$, will hold. In order for this to be true, the size of the plasma must be much larger than the Debye length, $L \gg \lambda_D = (\frac{\epsilon_0 k_B T_e}{ne^2})^{1/2}$, which is a measure of the shielding distance of a charge. In order for there to be collective behaviour, the number of particles within a Debye length from a charge must be large, $N_D = \frac{4\pi n \lambda_D^3}{3} \gg 1$ and the electromagnetic forces must be more important than the hydrodynamic forces. This means that the typical plasma oscillations must be faster than the collision frequency with neutral atoms, $\omega\tau > 1$, where ω is the frequency of a plasma oscillation and τ is the mean time between collisions.

In order for a fusion power plant to be useful, it must output at least as much energy as is put in, a condition called break-even. Ignition is the point at which all external heat sources can be turned off so that the temperature can be maintained solely from the energy of the α-particles from the fusion reactions. The energy released in the fusion reaction will be divided up between the α-particle and the neutron according to the mass so that the momentum is conserved in the collision. Hence about 80 % of the energy will be deposited on the neutron and lost from the plasma. A condition for ideal ignition where the presence of impurities in the plasma is neglected is $n_e \tau_E^* T = \frac{12 k_B T^2}{\langle \sigma v \rangle E_\alpha (1+5/Q)}$, here τ_E^* is the global energy confinement time, the total thermal energy content of the plasma divided by the lost power including radiation, $\langle \sigma v \rangle$ is the velocity averaged cross section of the fusion reaction, E_α is the energy of an α-particle and Q is the ratio of the fusion power produced to the heating power supplied. This is the so-called fusion triple product. It is used to characterize the performance of a fusion device as it combines $n_e \tau_E^*$, a measure of the merit of confinement called the Lawson criterion, with the temperature, which must also be sufficiently high to optimize fusion reactivity. The fusion triple product needed for three different Q-values is shown in Figure 2.1.

With the every tokamak constructed, the fusion triple product has doubled on average every 1.8 years, faster than "Moore's law" for the number of transistors in a microprocessor [20]. The JT60U Tokamak in Japan currently holds the record for the largest fusion triple product

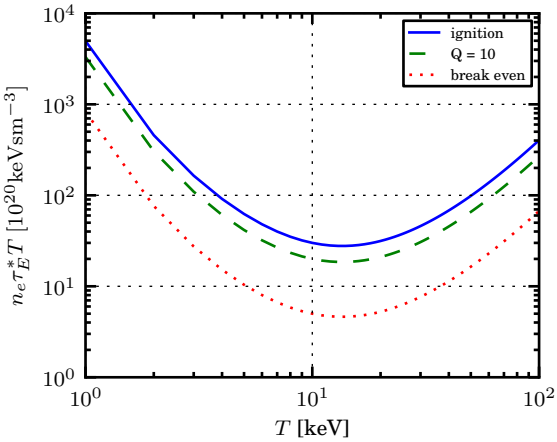

Figure 2.1: Fusion triple product versus temperature for the DT reaction, fusion cross section data from [21].

while the Joint European Torus (JET) in the UK has produced the largest fusion power, 16 MW, which corresponded to a Q value of 0.65. The next step is the construction of ITER in Cadarache in France. The goal of ITER is to produce 500 MW of output power with a Q-value of 10 for a duration of up to 480 seconds.

2.1 The tokamak

The Lorentz force $\mathbf{F} = q\mathbf{v} \times \mathbf{B}$, makes charged particles travel in helical orbits around the magnetic field lines. The radius of the gyration, the Larmor radius, is $\rho = \frac{mv_\perp}{|q|B}$ and thus much smaller for the electrons than for the ions, $v_\perp$ is the velocity of the particle perpendicular to the magnetic field lines. The frequency of this gyration, the cyclotron frequency, is $\omega_c = qB/m$. Sans collisions and turbulence, the particles' guiding centres would stay tied to to the field lines but remain free to move along them. The most obvious way to avoid losses of particles at the end of the magnetic field lines is to connect them in a toroidal configuration. This toroidal field can be produced by poloidal currents in coils external to the plasma. This toroidal field will go as $B_\phi \propto \frac{1}{R}$ where R is the radial distance from the centre of the tokamak.

However, particles following the field lines in such a configuration will be subject to drifts caused by the gradient of the magnetic field

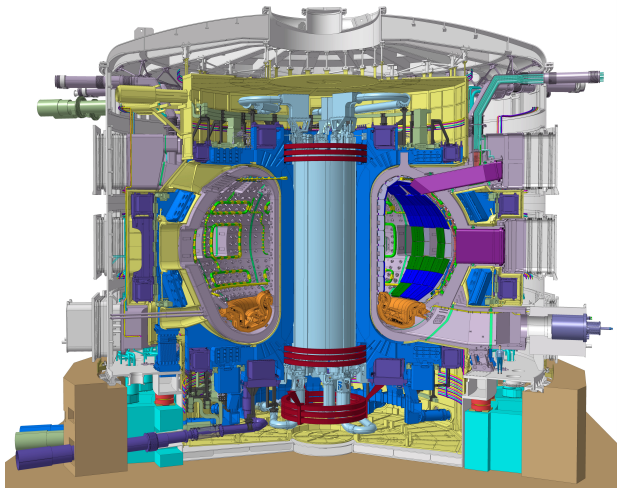

Figure 2.2: A cutaway of the ITER tokamak, which when finished will be the largest tokamak in the world. Image: ITER Organization.

strength and the curvature of the field lines. The ∇B drift is caused by the fact that the Larmor radius will be smaller where the magnetic field strength is larger. It is given by $\mathbf{v}_{\nabla B} = \frac{1}{2}\frac{mv_\perp^2}{qB}\frac{\mathbf{B}\times\nabla B}{B^2}$. The drift due to the curvature of the magnetic field lines and the centrifugal force is given by $\mathbf{v}_c = \frac{mv_\parallel^2}{qB}\frac{\mathbf{B}\times\nabla B}{B^2}$ [22]. Because of the dependence on the charge, these drifts will be in different directions for the electrons and the ions, creating a vertical electric field. This in turn will lead to an $\mathbf{E}\times\mathbf{B}$ drift according to $\mathbf{v}_E = \frac{\mathbf{E}\times\mathbf{B}}{B^2}$ that will cause both the electrons and ions to drift together, since the $\mathbf{E}\times\mathbf{B}$ drift is neither dependent on mass nor charge, radially outwards. The solution to this is to introduce a twist in the magnetic field lines by giving the field a poloidal component, B_θ. Then, the field lines will trace out nested surfaces, so-called flux surfaces. In a tokamak, the poloidal field is achieved by driving a current through the plasma. This is done by inducing a toroidal electric field by transformer action, that is, a flux change is generated through the torus. The current will then create the magnetic field through Ampere's law. The helical twist then compensates the toroidal drift as particles will spend time both on the inside and the outside of the device. A cutaway of the ITER tokamak showing the toroidal and poloidal field magnets as well as the central solenoid is shown in Figure 2.2.

The condition for equilibrium is that the force on the plasma must be zero everywhere, that is, the magnetic force must balance the force

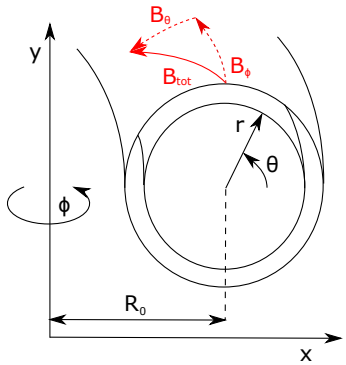

Figure 2.3: Toroidal geometry with two nested flux surfaces.

due to the plasma pressure,

$$\mathbf{j} \times \mathbf{B} = \nabla p. \tag{2.1}$$

It follows that $\mathbf{B}\cdot\nabla p = 0$ so that the flux surfaces are surfaces of constant pressure, it also follows that $\mathbf{j}\cdot\nabla p = 0$ and thus that the current lines also lie in the flux surfaces. The safety factor is a measure of how twisted the field lines are, and can be approximated as $q = \frac{rB_\phi}{R_0 B_\theta}$ in the circular limit. The safety factor can differ from flux surface to flux surface, the minimum is often near the magnetic axis with an increase outwards. The measure of how much the safety factor changes from flux surface to flux surface is the magnetic shear, $\hat{s} = \frac{r}{q}\frac{dq}{dr}$. If the cross section is circular, it is determined by the toroidal current density.

In general, the magnetic geometries in tokamaks are not circular, which makes it convenient to introduce flux functions that are constant on a flux surface, instead of relying on r. One such flux function is the poloidal magnetic flux function, ψ which is determined by the poloidal flux within each flux surface [22]. Flux surfaces and the commonly used coordinate system in a toroidal geometry is shown in Figure 2.3.

The equilibrium equation, Eq. 2.1, can for an axisymmetrical plasma be written as a differential equation dependent on two arbitrary functions of the poloidal flux function, $p(\psi)$ and $f(\psi)$ as

$$R\frac{\partial}{\partial R}\frac{1}{R}\frac{\partial \psi}{\partial R} + \frac{\partial^2 \psi}{\partial z^2} = -\mu_0 R^2 p'(\psi) - \mu_0^2 f(\psi) f'(\psi),$$

where $'$ denotes the derivative with respect to the poloidal flux. This is the Grad-Shafranov equation [22]. Numerical solutions to this equation

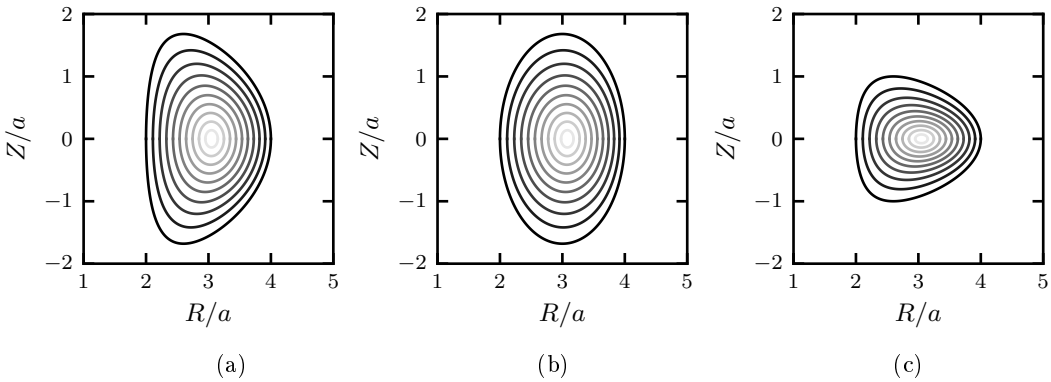

Figure 2.4: Shape of plasma cross sections illustrating the concepts of triangularity and elongation. The cross section in (a) has triangularity and elongation similar to that of a typical JET plasma, $\kappa = 1.4$, $\delta = 0.1$ at $r/a = 0.5$, while the cross section in (b) is just elongated and the one in (c) just exhibits triangularity.

are used in many simulation codes as well as different parametrizations. One such tokamak equilibrium model is the Miller model in which an expansion of the Grad-Shafranov equation is made, local to a flux surface, in terms of nine parameters. These parameters are the safety factor and magnetic shear, as well as the aspect ratio ($\varepsilon = r/R$), the pressure gradient (α), the elongation (κ), and triangularity (δ), and the radial variation of κ, δ, and R [23]. These equilibrium parameters are important to the stability of the microturbulence, as investigated in paper A. The elongation is one of the factors commonly used in the empirical scaling laws of the energy confinement time [24]. How elongation and triangularity affect the plasma cross section is shown in Figure 2.4.

2.2 Impurities

Impurities, which are here defined as any ion that is not a reactant in the fusion reaction, are detrimental to the performance of fusion devices in several ways. They dilute the plasma, lowering the output power and they can also cool the plasma through radiation. Heavy impurities might not be stripped of all their electrons. If the remaining electrons are excited, they emit photons of specific frequencies when they once

again are de-excited, so called line radiation.

There are several sources of impurities in tokamaks, they might be injected for control purposes or in order to decrease the power load on the plasma facing components. Impurities can also be released through the interaction of hot particles with the wall. For this reason, tokamak walls are often coated with light elements such as carbon, or beryllium, the coating foreseen for ITER and tested with the new ITER-like wall at JET. However, the power densities at the divertor, where the magnetic field lines are in contact with the vessel, will be even higher at around $10\,\mathrm{MWm}^{-2}$, requiring materials with higher meting points such as tungsten.

The third source of impurities are the fusion reactions themselves. The resulting thermalised helium must be transported out of the plasma sufficiently rapidly. How, and at what rates the impurities are transported, inwardly or outwardly, during different conditions, is thus of great importance since strong inward transport of a heavy impurity like tungsten might be lethal to the discharge. This is investigated in papers A and B.

Chapter 3

Transport theory

In order to achieve fusion power economically, the fusion triple product, $n_e \tau_E^* T$, must be maximized, here n_e is the electron temperature, τ_E^* is the energy confinement time, and T is the temperature. However, the temperature and density are constrained respectively by the need to maximize the fusion cross-section and maintaining global stability. The stability constraint on the density is the so called Greenwald limit, an empirical result that limits the plasma density to $\bar{n}/10^{20} = \kappa J$, where κ is the elongation and J is the average current density in MA/m^3 [22]. The temperature and density is also constrained by the β limit, β is the ratio of the plasma pressure to magnetic pressure, $\beta = \frac{nT}{B^2/(2\mu_0)}$. If the plasma pressure becomes too large compared to the magnetic pressure, large scale magnetohydrodynamic instabilities, such as ballooning modes, will occur. A high β value is important from an economic standpoint since the fusion power scales as n^2 while the strength of the confining magnetic field is a large factor in the cost of the device.

Hence, the only avenue to improve the fusion triple product is to increase the energy confinement time, τ_E^*. The energy confinement time is connected to the radial transport of particles and energy. The transport depends on a number of processes, from sawteeth in the centre of the plasma to edge localized modes (ELMs) towards the edge. Aside from these intermittent phenomena, the transport is determined by local processes whereby the particles undergo diffusion and convection. Diffusion is the net movement of a quantity from a region of high concentration down a concentration gradient. It can be explained by the random walk processes the particles undergo. Convection, on the other hand, is a collective movement of particles. The net convective velocity, the so-called

pinch, of a species can have the opposite sign of the diffusion so that an inwardly peaked profile can be sustained in steady state.

It was long believed that the transport in tokamaks could be described by the Coulomb interactions alone as in classical and neoclassical theory. However, it was soon realized that the heat and particle transport observed were up to two orders of magnitude larger [25]. The so called "anomalous" transport make up the rest and thus dominate over the neoclassical transport. It has long been accepted that turbulent transport explains this degradation in confinement. The transport can be both due to instabilities that let the particles escape their flux surfaces or lead to the break-up of the flux surfaces themselves. The main candidate for the turbulent transport is turbulence due to small scale instabilities driven by the very steep gradients in density and temperature, referred to as microinstabilities, as discussed in Section 3.4.

3.1 Kinetic approach

Collisions can be rare in high-temperature plasmas and the velocity distributions of the species might therefore remain non-Maxwellian for a long time. A kinetic description is then needed and because of the large number of particles involved, it can be statistical. A distribution function for each species in phase space, $f_j(t, \mathbf{r}, \mathbf{v})$, can then be used. Without collisions, the change of the distribution function is expected to be zero in the frame moving with the particles, $\frac{\mathrm{d}f}{\mathrm{d}t} = 0$. Writing out this total derivative for particle j, we have

$$\frac{\mathrm{d}f_j}{\mathrm{d}t} = \frac{\partial f_j}{\partial t} + \frac{\partial f_j}{\partial x}\frac{\partial x}{\partial t} + \frac{\partial f_j}{\partial y}\frac{\partial y}{\partial t} + \frac{\partial f_j}{\partial z}\frac{\partial z}{\partial t} + \frac{\partial f_j}{\partial v_x}\frac{\partial v_x}{\partial t} + \frac{\partial f_j}{\partial v_y}\frac{\partial v_y}{\partial t} + \frac{\partial f_j}{\partial v_z}\frac{\partial v_z}{\partial t} = 0,$$

which can be written as

$$\frac{\partial f_j}{\partial t} + \mathbf{v} \cdot \nabla f_j + \mathbf{a} \cdot \frac{\partial f_j}{\partial \mathbf{v}} = 0.$$

With Newton's third law $\mathbf{F} = m_j \mathbf{a}$, where m_j is the mass of species j, and the force on a particle from an electromagnetic field $\mathbf{F} = e_j(\mathbf{E} + \mathbf{v} \times \mathbf{B})$, where e_j is the charge of species j and $\mathbf{E}$ and $\mathbf{B}$ are the total electric and magnetic fields, we get

$$\frac{\partial f_j}{\partial t} + \mathbf{v} \cdot \nabla f_j + \frac{e_j}{m_j}(\mathbf{E} + \mathbf{v} \times \mathbf{B}) \cdot \frac{\partial f_j}{\partial \mathbf{v}} = 0, \tag{3.1}$$

which is the Vlasov equation. However, the cumulative effect of multiple small angle collisions are often important in magnetized fusion plasmas since the range of the Coulomb interaction in principle is infinite. Adding a collision term, we get the Boltzmann equation [22],

$$\frac{\partial f_j}{\partial t} + \mathbf{v} \cdot \nabla f_j + \frac{e_j}{m_j}(\mathbf{E} + \mathbf{v} \times \mathbf{B}) \cdot \frac{\partial f_j}{\partial \mathbf{v}} = \left(\frac{\partial f}{\partial t}\right)_c . \tag{3.2}$$

The collisional particle interactions are effectively random and the collision operator provides a statistical account of this. It represents the effects of soft collisions, each only making a small change in the particles' velocities [25]. In this work, the collision operator used is the linearised Landau-Boltzmann operator.

The electric and magnetic fields in Eq, 3.2 are determined by Maxwell's equations that couple back to 3.2 through the charge density ρ_j and current densities $\mathbf{j}_j$, which are obtained by taking velocity moments of the particle distribution function. Maxwell's equations,

$$\begin{aligned} \nabla \cdot \mathbf{E} &= \sum_j \frac{\rho_j}{\epsilon_0} \\ -\mu_0 \epsilon_0 \frac{\partial \mathbf{E}}{\partial t} + \nabla \times \mathbf{B} &= \sum_j \mu_0 \mathbf{j}_j \\ \nabla \cdot \mathbf{B} &= 0 \\ \nabla \times \mathbf{E} + \frac{\partial \mathbf{B}}{\partial t} &= 0, \end{aligned}$$

together with the Fokker-Planck equation completely describes a plasma self-consistently. However, numerical solutions are expensive because of the dimensionality of $f_j(t, \mathbf{r}, \mathbf{v})$, so simplifications are necessary; like the fluid approach where the dimensionality is reduced by three as discussed in Section 3.2 or gyrokinetic theory where the dimensionality is reduced by one, as discussed in Chapter 4.

3.2 Fluid approach

It is often enough to describe a plasma in terms of fluid quantities such as the particle density, $n(t, \mathbf{x})$, the fluid velocity, $\mathbf{u}(t, \mathbf{x})$ and the pressure, $p(t, \mathbf{x})$ which are functions of just four variables instead of the seven of the kinetic distribution function. The fluid equations can be derived by taking moments of the Fokker-Planck equation. If Eq. 3.2 is multiplied

by 1, $m\mathbf{v}$ and $\frac{1}{2}mv^2$ and integrated in velocity space, the result is the continuity equation which describes the evolution of density,

$$\frac{\partial n}{\partial t} = -\nabla \cdot (n\mathbf{u}),$$

the fluid equation of motion which describes the evolution of momentum,

$$\frac{\partial}{\partial t} mn\mathbf{u} = en(\mathbf{E} + \mathbf{u} \times \mathbf{B}) - \nabla \cdot \mathbf{P} + \mathbf{F},$$

where $\mathbf{F}$ is the friction force, given by $\mathbf{F} = \int m\mathbf{v}Cd^3v$ where C is the collision operator and $\mathbf{P} = \int m\mathbf{v}\mathbf{v}fd^3v$ is the pressure tensor, and the energy equation, describing the evolution of pressure,

$$\frac{\partial}{\partial t}\left(\frac{3}{2}p + \frac{1}{2}mn\mathbf{u}^2\right) + \nabla \cdot \mathbf{Q} = W + \mathbf{u} \cdot (\mathbf{F} + en\mathbf{E})$$

where $\mathbf{Q} = \frac{1}{2}mv^2\mathbf{v}fd^3v$ is the energy flux and $W = \int \frac{1}{2}m(\mathbf{v} - \mathbf{u})^2 Cd^3v$ is the energy exchange [25]. The evolution of the energy flux is then obtained by taking one further moment of Eq. 3.2, and so on. This procedure will not lead to a closed set of equations and the resulting hierarchy must be truncated. In the Chalmers fluid model, used in this work, the hierarchy is truncated at the diamagnetic heat flow with $\mathbf{q}^* = \frac{p}{m\omega_c}\frac{\mathbf{B}\times\nabla T}{B}$ [26].

3.3 Neoclassical transport

Classical transport is the irreducible transport due to collisions. If the effects of a toroidal geometry is added, the transport is known as neoclassical. From Ohm's law $\mathbf{E} + \mathbf{v} \times \mathbf{B} = \eta\mathbf{j}$, where η is the resistivity tensor with the value $\eta_\parallel$ for the current parallel to the magnetic field and $\eta_\perp$ perpendicular, and the pressure balance equation $\mathbf{j} \times \mathbf{B} = \nabla P$ from single-fluid MHD theory, the velocity perpendicular to the magnetic field can be derived as

$$\mathbf{v}_\perp = \frac{\mathbf{E} \times \mathbf{B}}{B^2} - \eta_\perp \frac{\nabla p}{B^2}. \tag{3.3}$$

With constant temperature and zero electric field, the flux will be $\Gamma_\perp = n\mathbf{v}_\perp = -\frac{\eta_\perp \beta}{2\mu_0}\nabla n$ where $\beta = \frac{nT}{B^2/2\mu_0}$ is the ratio of pressure to the magnetic pressure. The diffusion coefficient is then, from Fick's law which relates the collisional flux to the density gradient,

$$\Gamma = -D\nabla n,$$

$D_\perp = \frac{\eta_\perp \beta}{2\mu_0}$, the classical diffusion coefficient for a fully ionized gas. A rough estimate for the resistivity is obtained if the electron collision time is assumed to be the same as the time for the momentum loss of the electrons when they collide with ions. The force due to the electric field is then balanced by the force due to collisions $Ee = \frac{m_e v}{\tau_e}$. The resistivity is defined by Ohm's law, $E = \eta v n e$ so that $\eta = \frac{m_e}{n_e e^2 \tau_e}$. A thorough calculation from the kinetic equation for the electron distribution function yields a result about half as large [22]. With this estimate, the diffusion coefficient will be same as if the diffusion was due to a random walk with a step size of the Larmor radius, $D \sim \frac{\rho_e^2}{\tau_e}$, where ρ_e is the electron Larmor radius.

The resistive diffusion in a toroidal plasma is more complicated due to a number of effects which depend on the collision frequency. If the collision frequency is low enough, particles trapped on the low field side of the torus will dominate the transport. The particles are trapped by the mirror force resulting from the fact that the magnetic moment of a particle is constant and that there will be a parallel force on a diamagnetic particle deaccelerating it while going towards higher magnetic field strengths. The particles will then execute banana orbits, so-called since they will trace out banana shaped orbits if viewed in a poloidal cross section. An estimate for the associated diffusion coefficient is then given by a random walk with a step length the same as the width of a banana orbit, given by $w_{be} \sim (q/\varepsilon^{1/2})\rho_e$ where ε is the inverse aspect ratio of the magnetic surface, $\varepsilon = r/R_0$. Since just a fraction of the particles $\sim \varepsilon^{1/2}$ will be trapped, the diffusion coefficient is given by $D \sim \frac{q^2}{\varepsilon^{3/2}} \frac{\rho^2}{\tau_e}$. In this banana regime, the inductive toroidal electric field will also give rise to a new inward flux, the so-called Ware pinch. The electric field will will displace the trapped particle orbit poloidally. Because of this, the ∇B and curvature drifts will not be symmetric about the midplane and the particles will experience an inward drift for longer than they experience an outward drift. The net pinch of the trapped particles is $\langle v_r \rangle \backsimeq -E_\parallel / B_\theta$, independent of charge or mass. Since the trapped particle fraction is $\sim \varepsilon^{1/2}$, the net radial flow goes as [27]

$$\Gamma_r^{Ware} \sim -\varepsilon^{1/2} \frac{E_\parallel}{B_\theta}.$$

If the collisionality is higher, trapping of particles on the low field side will be negligible. Pfirsch-Schlüter diffusion will then be important. It is a result of the outward hoop force that arises due to the toroidal

geometry of the plasma. A vertical current is then needed to balance this force. The current is returned by flowing along the magnetic field lines, this is the so-called Pfirsch-Schlüter current [22]. From Eq. 3.3 it is evident that this current will give rise to a perpendicular flow through the parallel electric field $E_\parallel = \eta_\parallel \mathbf{j}_\parallel$. While the fluxes of energy and main ions due to neoclassical effects are typically negligible compared to the turbulent transport, it can have an important effect on heavy impurities, especially if their distribution is poloidally asymmetric [28].

3.4 Turbulent transport and microinstabilities

The class of instabilities which have a wavelength close to the ion Larmor radius are called microinstabilities. This type of instabilities does not interrupt the discharge, like larger scale magnetohydrodynamic (MHD) instabilities might do, but the small scale random advection they cause will impact plasma confinement. There are many types of microinstabilities, both electrostatic and electromagnetic. They will create fluctuations in the electric field and thus produce an $\mathbf{E} \times \mathbf{B}$ drift velocity according to $\delta v_\perp = \frac{\delta E}{B}$. If there is also a density fluctuation that is not completely out of phase with $\delta v_\perp$ there will be a convective particle flux through

$$\Gamma_j = \left\langle \delta v_{\perp_j} \delta n_j \right\rangle,$$

where the average is over a flux surface. If the turbulence is electromagnetic and thus also gives rise to fluctuations in the magnetic field, $\delta\mathbf{B}$, that also causes a radial particle flux given by

$$\Gamma_j = \frac{n}{B} \left\langle \delta v_{\parallel_j} \delta B_r \right\rangle.$$

This turbulent transport can be described in terms of effective diffusivity and pinches when averaging over time and space. Similarly, fluctuations in temperature give rise to heat fluxes. The fluxes can be divided into different terms depending on different driving gradients. For the particle flux we get

$$\frac{R\Gamma_j}{n_j} = D_j \frac{R}{L_{n_j}} + D_{T_j} \frac{R}{L_{T_j}} + D_u \frac{R}{L_u} + RV_{p,j}, \tag{3.4}$$

here R is the major radius of the tokamak, and R/L_{X_j} is the normalized inverse gradient scale length of the quantity X. The first term on the right hand side is ordinary diffusion, the second is thermodiffusion

and the third roto-diffusion. $V_{p,j}$ is the convective velocity of species j. Impurities with low concentration, trace impurities, will not affect the over-all turbulence. Hence, the impurity gradients will not affect the impurity diffusion coefficients or the pinch velocity, so Eq. 3.4 will be linear. Of great importance is the steady state density gradients of main ion and impurities since they determine, for example, whether impurities will be accumulated in the core. If the last three terms in Eq. 3.4 is collected into a total pinch V_j and the equation solved for zero particle flux, i.e. with no sources or sinks of particles other than at the edge, the definition of the so-called peaking factor is obtained,

$$PF_j = \frac{R}{L_{n_j}} = -\frac{RV_j}{D_j}.$$

This is the steady state density gradient of zero particle flux for species j. A positive peaking factor means that the density profile is peaked, hence the name, necessitating an inward net particle pinch. Conversely, if the peaking factor is negative, there is a net outward pinch, which is desirable for impurities.

The instabilities are characterized by the critical gradients in density and temperature over which they are destabilized. Small fluctuations can often be assumed in the core of the plasma, $\frac{\delta n}{\langle n \rangle} \ll 1$, so the system of equations describing the plasma can be linearised with i.e. $n = \langle n \rangle + \delta n$ and a Fourier description used for the modes $\delta n \sim \exp i(\mathbf{k} \cdot \mathbf{r} - \omega t)$. A dispersion relation relating the wave vector $\mathbf{k}$ to the frequency $\omega = \omega_r + \gamma$, where ω_r is the real frequency and γ the growth rate can then be obtained. The critical gradient thresholds can then be determined for when the mode is unstable, $\gamma > 0$. These instabilities will grow until they are large enough so that the linear assumptions will not hold, the different modes will couple to each other and enter into the non-linear regime. A saturation amplitude of the fluctuations then needs to be determined in order to calculate the level of transport.

Zonal flows are an important saturating mechanism. They are poloidally symmetric, linearly stable modes that provide flow shear and draw energy from the unstable drift waves. The perpendicular scale length of the microinstabilities are on the order of several gyroradii as the average amplitude of the fluctuation seen by a particle would be averaged out as the scale length approaches the Larmor radius.

3.4.1 Drift waves

Drift instabilities are often said to be the cause of the anomalous transport in tokamaks. They are electrostatic and are driven by the free energy in density and electron temperature. They develop from the electron drift wave which can propagate in a plasma slab with a shearless, uniform magnetic field. A wave travelling in the y direction, $\delta n \exp i(k_y y - \omega t)$, has a surface of constant density as indicated in Figure 3.1. Because of the high speed and low inertia of the electrons, a common approximation is to say that they are free to move along the field lines. The force balance will be given by $ne\mathbf{E}_{\|} + \nabla p_e = 0$ which linearised leads to the Boltzmann response for the electron density,

$$\frac{\delta n_e}{n_e} = \frac{e\delta\varphi}{T_e}. \tag{3.5}$$

Thus, a perturbed density will lead to a perturbed electrostatic potential and there will be an electric field pointed from the area of increased density to the area of decreased density. This will cause an $\mathbf{E} \times \mathbf{B}$ drift that will serve to increase the density in less dense regions and increase it in more dense areas, thus causing the density and potential perturbations to oscillate. This wave, the drift wave, will travel in the y direction. By using the quasineutrality condition $\delta n_e = \delta n_i$ and the linearised continuity equation for the ions $\mathrm{i}\omega\delta n_i = \delta v_{\mathbf{E}\times\mathbf{B}} \frac{dn}{dx}$ where the $\mathbf{E} \times \mathbf{B}$ velocity is given by $\delta v_{\mathbf{E}\times\mathbf{B}} = -\frac{1}{B}\frac{\partial\delta\varphi}{\partial y}$ the frequency becomes

$$\omega = -\frac{k_y T_e}{eBn}\frac{\mathrm{d}n}{\mathrm{d}r},$$

which is the electron diamagnetic frequency, ω_{*e}.

However, since the density and potential perturbations are in phase, this will not lead to any net transport across the flux surfaces, for that, electron dissipation needs to be introduced through collisions or Landau damping. However, some modes, like the ITG mode, are reactive instead of dissipative and do not require dissipation in order to grow. As discussed in Section 3.3, particles in a tokamak can be either trapped on the low field side or passing, giving rise to different dynamics and modes. Two of the most important electrostatic modes from each category are discussed in the following sections.

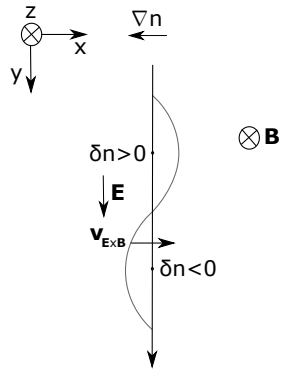

Figure 3.1: Illustration of a drift wave in a slab with a homogeneous magnetic field in the z direction and the wave of constant density travelling in the y (poloidal) direction. Adapted from [22].

3.4.1.1 Ion temperature gradient mode

The ion temperature gradient mode is the most likely driver of ion and electron heat transport in the core of tokamaks [24]. For a qualitative treatment of the ITG mode, trapped particle effects can be neglected, since the frequency of the mode is much larger than that of the bounce frequency, $\omega \gg \omega_{b,j}$. An adiabatic Boltzmann electron density response can also be assumed, $k_\parallel v_{Te} \gg \omega \gtrsim k_\parallel v_{Ti}$. An important parameter is η_i, the ratio of the density scale length to the temperature scale length, which is why the mode is often referred to as an η_i mode. The ITG mode is excited when this parameter exceeds a critical value $\eta_{ic} \sim 1$ [29]. Two branches can be identified depending on whether the toroidal coupling is important or not. If it is weak, the so-called slab branch can be excited with $\omega \sim (k_\parallel^2 v_{Ti}^2 \omega_{*i} \eta_i)^{1/3}$ [30] where $k_\parallel$ is the wave vector parallel to the magnetic field, v_{Ti} is the thermal velocity of the ions and ω_{*i} is the ion diamagnetic frequency.

In a torus on the low field side, the toroidal branch with $\omega \sim (\eta_i \omega_{*i} \omega_{di})^{1/2}$, where $\omega_{di} = \mathbf{k} \cdot \mathbf{v}_d$ is the ion magnetic drift frequency, usually dominates [22]. This is because, in this bad-curvature region, the magnetic field gradient, curvature vector and temperature gradient are all in the same direction. The mechanism behind the bad-curvature driven ITG mode is illustrated in Figure 3.2. A drift wave is set up in the region between the hot and cold plasma. Since the ∇B and curvature drifts are proportional to temperature, the difference in the magnetic drift velocity of the ions will set up an electric field, which will cause an $\mathbf{E} \times \mathbf{B}$ drift

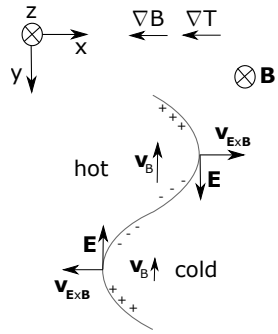

Figure 3.2: The Rosenbluth-Longmire picture of the bad-curvature driven ITG instability.

that amplifies the original perturbation. The instability is similar to the Rayleigh-Taylor instability, which occur when a lighter fluid is pushing a heavier fluid. An example is when a denser fluid is supported by a less dense fluid under the influence of gravity. On the high field side the directions of ∇B and ∇T are opposite, so the $\mathbf{E} \times \mathbf{B}$ drift will also be opposite, thus suppressing the original perturbation. Because of this, the perturbations will have their maxima on the outboard side and their minima on the inboard side. Perturbations with this poloidal structure are referred to as ballooning.

3.4.1.2 Trapped electron mode

Particles that are trapped in the low field region of the torus behave differently than the passing particles in that they average out the parallel velocity over a bounce period. They do not go around the whole torus poloidally or toroidally, so the curvature drift is not averaged out. This gives rise to several trapped particle modes on the outboard side of the tokamak. The trapped electron mode has two regimes dependent on whether collisions are important for the instability to arise or not, dissipative (DTEM) and collisionless (CTEM).

The collisionality needs to be small enough so that the trapped particles are not scattered into passing orbits. If this is the case, and η_i is small enough so that the ITG mode is not excited, the TE mode can dominate. The physical picture of the collisionless trapped electron mode is that the curvature drift, which is in different directions for ions end electrons, create a charge polarization, resulting in an $\mathbf{E} \times \mathbf{B}$ flow that

Instability	Source of free energy	Branch	Properties
ITG	∇T_i	Slab	$\omega \leq \omega_{*i}$, $\eta_i > \eta_{ic}$
		Toroidal	$\eta_i > \eta_{ic}$
TEM	∇T_e,∇n	Dissipative	$\varepsilon\omega < \nu_e \leq \varepsilon^{3/2} v_{th}/qR$, $L_n q/R < k_\perp \rho_s \leq \nu_e L_n/\varepsilon c_s$
		Collisionless	$\nu_e < \varepsilon\omega \leq \varepsilon^{3/2} v_{th}/qR$, $L_n q/R < k_\perp \rho_s \leq 1$

Table 3.1: Properties of some microturbulence modes. ω_{*i} is the ion diamagnetic frequency, ρ_s is the ion Larmor radius, c_s is the sound speed and L_n is the density scale length. [31]

enhances an initial density perturbation. In the large aspect ratio limit with $T_i = T_e$ the complex mode frequency is $\omega^2 = \bar{\omega}_{de}(\bar{\omega}_{de} + \sqrt{2\varepsilon}\omega_{*e})$ [22], where over-bar denote bounce averaging. In contrast to the ITG mode, the trapped electron modes propagate in the direction of the electron diamagnetic frequency. The main drive is the electron temperature and density gradients. Properties of these microturbulence modes are summarized in Table 3.1.

Chapter 4

Gyrokinetic theory

The basis of gyrokinetic theory is the assumption that the particles' gyromotion around the magnetic field lines is much faster than the frequencies of the electrostatic or electromagnetic fluctuations of interest. This fast orbital motion can then be averaged over and instead of following the trajectories of the particles, the trajectories of the resulting "charged rings" are followed. Any dependence of the gyroangle, θ, can then be removed. In that way, the number of dimensions is reduced by one and the timestep can be increased past the gyroperiod, which greatly reduces the computational cost.

Nonlinear gyrokinetic simulations are important in the study of low-frequency plasma turbulence and its transport and can be used to simulate a number of instabilities such as the aforementioned ITG and TE modes as well as the trapped ion mode, electron temperature gradient mode, drift-Alfvén turbulence, microtearing and drift-tearing mode and energetic particle driven MHD instabilities [32].

It has been observed that the fluctuations in magnetically confined high-temperature plasmas are typically broadband ($\Delta\omega \sim \omega_k$) with frequencies and wavelengths similar to those of drift-wave theories, $\omega = \omega_*$, with typical fusion plasma parameters $\omega_*/\omega_c \sim 10^{-3}$. The turbulent diffusion coefficient from a random walk argument is $D \sim \frac{(\Delta r)^2}{\Delta t} \sim \frac{\Delta\omega}{k_r^2} \sim \frac{\omega_*}{k_r^2}$. If the wavelength is similar to the ion gyroradius $k_r \propto 1/\rho_i$, the gyro-Bohm scaling is obtained, $D \sim \frac{\rho_i}{L}\frac{T}{eB}$.

The derivation of the gyrokinetic Vlasov-Maxwell equations relies on the existence of small ordering parameters. The Larmor radius needs to be small compared to the scale lengths of the background magnetic field, L_B, and gradient scale lengths of the background density and temper-

ature, $\epsilon_B = \rho_i/L_B \ll 1$. Furthermore, the cyclotron frequencies need to be much larger than the frequencies of the turbulent fluctuations, $\frac{\omega}{\omega_c} \sim \epsilon_\omega \ll 1$. The wavelength of the turbulence cannot be assumed to be large compared to the Larmor radius and full finite-Larmor-radius effects must be retained so that strong wave-particle interactions are captured, $|\mathbf{k}_\perp|\,\rho_i = \epsilon_\perp \sim 1$. The fast motion of particles along the field lines compared to the drift velocity across field lines means that the parallel wavelength of the turbulence is much larger than the perpendicular ditto, $\frac{|k_\parallel|}{|\mathbf{k}_\perp|} \sim \frac{\epsilon_\omega}{\epsilon_\perp}$. Furthermore, the amplitude ordering parameter ϵ_δ dictates that the amplitude of the fluctuating part of the distribution function, electric, and magnetic field must be small, $\left|\frac{\delta f}{F}\right| \sim \frac{|\delta \mathbf{E}_\perp|}{B v_{th}} \sim \epsilon_\delta \ll 1$. This implies that the energy associated with the turbulence is small compared to the thermal energy, $\frac{e\delta\phi}{T} \sim \epsilon_\delta$. The ordering parameters for the background, the fluctuating fields and the amplitude are often comparable in practice [32] ($\epsilon_B \sim \epsilon_\omega \sim \epsilon_\delta \sim 10^{-3}$) giving the gyrokinetic ordering

$$\epsilon \sim \frac{\rho_i}{L_B} \sim \frac{\rho_i}{L_F} \sim \frac{\omega}{\omega_c} \sim \frac{k_\parallel}{k_\perp} \sim \frac{e\delta\phi}{T} \ll 1.$$

Instead of studying the the evolution of the distribution function of the particles, $f(t, \mathbf{r}, \mathbf{v})$, the evolution of the gyrocenter distribution in gyrocenter phase space $F(t, \mathbf{X}, v_\parallel, \mu)$, is studied, $\mathbf{X}$ is the gyrocenter position, $v_\parallel$ is the gyrocenter parallel velocity and $\mu = m v_\perp^2/(2B)$ is the magnetic moment. The Vlasov equation (3.1) in these coordinates then becomes

$$\frac{\mathrm{d}F}{\mathrm{d}t} = \frac{\partial F}{\partial t} + \frac{\mathrm{d}\mathbf{X}}{\mathrm{d}t} \cdot \nabla F + \frac{\mathrm{d}v_\parallel}{\mathrm{d}t}\frac{\partial F}{\partial v_\parallel} + \frac{\mathrm{d}\mu}{\mathrm{d}t}\frac{\partial F}{\partial \mu} = 0 \tag{4.1}$$

which states that the gyrocenter Vlasov distribution is constant along a gyrocenter orbit in gyrocenter phase space. The fields are decomposed into their background and fluctuating parts, $\Phi(\mathbf{x}) \to \Phi_0(\mathbf{x}) + \Phi_1(x)$, $\mathbf{A}(\mathbf{x}) \to \mathbf{A}_0(\mathbf{x}) + \mathbf{A}_1(\mathbf{x})$. The $\mathbf{E} \times \mathbf{B}$ drift, ∇B-drift and curvature drift are given in Gaussian units by

$$\begin{aligned}
\mathbf{v}_\chi &= -\frac{c}{B_0^2}\nabla\chi_1 \times \mathbf{B}_0 \\
\mathbf{v}_{\nabla\mathbf{B}} &= \frac{\mu}{m\omega_c}\mathbf{b}_0 \times \nabla B_0 \\
\mathbf{v}_c &= \frac{v_\parallel^2}{\omega_c}(\nabla \times \mathbf{b}_0)_\perp
\end{aligned}$$

where χ_1 is the modified potential $\chi_1 = \bar{\Phi}_1 - \frac{v_\parallel}{c}\bar{A}_{1\parallel} + \frac{1}{q}\mu\bar{B}_{1\parallel}$ and where the over-bar denote gyroaveraging and $\mathbf{b}_0$ denote the unit vector pointing in the direction of $\mathbf{B}_0$. The assumption is made that the amplitudes of the perturbed fields are much smaller than the background fields, and then the time derivatives of the coordinates are

$$\begin{aligned}
\frac{\mathrm{d}\mathbf{X}}{\mathrm{d}t} &= v_\parallel \mathbf{b}_0 + \frac{B_0}{B^*_{0\parallel}}(\mathbf{v}_\chi + \mathbf{v}_{\nabla B} + \mathbf{v}_c) \\
\frac{\mathrm{d}v_\parallel}{\mathrm{d}t} &= \left(\frac{\mathbf{b}_0}{m} + \frac{B_0}{m v_\parallel B^*_{0\parallel}}(\mathbf{v}_\chi + \mathbf{v}_{\nabla B} + \mathbf{v}_c)\right) \cdot \\
&\quad \cdot \left(-q\nabla\bar{\Phi}_1 - \frac{q}{c}\mathbf{b}_0\frac{\mathrm{d}\bar{A}_{1\parallel}}{\mathrm{d}t} - \mu\nabla(B_0 + \bar{B}_{1\parallel})\right) \\
\frac{\mathrm{d}\mu}{\mathrm{d}t} &= 0.
\end{aligned}$$

Inserting these into Eq. 4.1, the standard formulation of the gyrokinetic Vlasov equation for species j is obtained, as in [33],

$$\begin{aligned}
&\frac{\partial F_j}{\partial t} + \left(v_\parallel \mathbf{b}_0 + \frac{B_0}{B^*_{0\parallel}}(\mathbf{v}_\chi + \mathbf{v}_{\nabla B} + \mathbf{v}_c)\right) \cdot \\
&\cdot \left(\nabla F_j + \frac{1}{m_j v_\parallel}\left(-q_j\nabla\bar{\Phi}_1 - \frac{q_j}{c}\mathbf{b}_0\frac{\mathrm{d}\bar{A}_{1\parallel}}{\mathrm{d}t} - \mu\nabla(B_0 + \bar{B}_{1\parallel})\right)\frac{\partial F_j}{\partial v_\parallel}\right) = 0
\end{aligned} \tag{4.2}$$

where $\mathbf{B}^*_0 = \nabla \times (\mathbf{A}_0 + \frac{mc}{q}v_\parallel \mathbf{b}_0)$.

The derivation of the gyrokinetic Vlasov equation can be done by a coordinate transform using Lie formalism after which the fast gyromotion of the particles can be integrated out as presented in [32]. In much the same way, the gyrokinetic field equations can be derived from Maxwell's equations using the same Lie generators. The gyrokinetic Maxwell equations together with the gyrocenter Vlasov equation then form a complete self-consistent set of equations. Since fast frequencies are removed, quasineutrality can be assumed so that, for a two-species plasma $q_i n_i = e n_e$. In order to model collisions, a collision operator must be added to the right hand side of Eq. 4.2. The Landau-Boltzmann operator, used in this work, ensures the conservation of particles, momentum and energy at each point in space. Another property is that of Boltzmann's

H-theorem which says that the entropy will increase until it reaches its maximum entropy state, a Maxwellian.

So called δf-codes separate the macroscopic evolution of the plasma from the microturbulence, $F_j \rightarrow F_{j0} + F_{j1}$ where the perturbed part is small compared to the background, $F_{j1}/F_{j0} \sim \epsilon$, while assuming that the background part is stationary [33]. This reduces the computational effort. It also simplifies the treatment of collision operators. The linearised form of the Landau-Boltzmann operator also ensures the conservation of particles, momentum and energy [34].

4.1 Flux tube

The magnetic equilibrium geometry has to be specified in order to solve the system of equations formed by the gyrokinetic Vlasov and Maxwell equations. The equations could be solved for the whole plasma volume, resolving the whole torus, a so-called global simulation. However, the domain can be reduced significantly if a flux tube domain is used. In this approximation, a field line is followed an integer number of poloidal turns around the torus. Since a tokamak, ignoring ripple effects from the external magnets, is axisymmetrical, all variations are sampled after one turn [35]. The simulation box is then a curved and sheared box around a central field line. This limits the simulations to local investigations, the background density and temperature and their radial gradient are taken to be constant across the radial extent. Since they are constant on a flux surface, their parallel dependence can be neglected. The flux tube approximation is valid as long as the background perpendicular length scales exceed the turbulence correlation lengths and the radial extent of the box is small compared to the machine size.

The magnetic geometry that contain the metric coefficients that determine the shaping of the box are taken as input. In this work analytical geometries such as $\hat{s}-\alpha$ and Miller equilibriums as well as numerical solutions to the Grad-Shafranov equation [36] are used. As touched upon before, the correlation lengths of the turbulence are much longer along, than perpendicular to, the field lines. Consequently, if a grid aligned coordinate system is used, the computational cost can be lowered by 2 - 3 orders of magnitude since the computational grid can be much coarser along the field lines. The coordinates are then the flux label, x, which is perpendicular to the flux surface, the direction parallel to the field lines, z, and the binormal direction, y, which labels the field lines on

the flux surface. Since the simulation domain does not cover the whole physical domain, the boundary conditions should be chosen as to minimize the effect of the reduction. In the radial and binormal direction, periodic boundary conditions are suitable, $F(x + L_x, y, z) = F(x, y, z)$, $F(x, y + L_y, z) = F(x, y, z)$, where L_x and L_y are the box sizes in the direction of x and y, respectively. This also ensures that particles and heat are conserved in the simulation box since losses due to radial fluxes are replenished, thus this choice of boundary conditions also allows for arbitrary long simulation times since there will be no profile relaxation. The periodic boundary conditions also allow for a Fourier representation in the perpendicular plane. In the parallel direction, pseudoperiodic conditions need to be used since, for a general safety factor, the ends of the simulation box which are at the same poloidal position, do not coincide toroidally. Since the turbulent fluctuations are largest at the low field side side, the matching of the ends are done on the high field side, in order to reduce the numerical effects of the boundaries. The parallel boundary condition is given by

$$F(k_x, k_y, \pi) = (-1)^{nN} F\left((m + nN)\frac{2\pi}{L_x}, k_y, -\pi\right)$$

where $m = k_x \frac{L_x}{2\pi}$, $n = k_y \frac{L_y}{2\pi}$, and N is the number of flux tubes needed to cover the torus [35].

4.2 Gyrokinetic simulations

A number of gyrokinetic codes exist that use either a particle-in-cell approach or solves the gyrokinetic equations on a fixed grid. The GENE[1] code [37], which is used in this work, belongs to the latter group. It is a δf code that can be used both in linear and nonlinear mode. Nonlinear mode is much more computationally expensive since it requires transformations back and forth between Fourier and real space, where the computation of the nonlinearity has to be performed. In linear simulations, the coupling between different turbulent modes is ignored, one mode is studied at a time. The transport will thus not saturate, but the growth rate and frequency of the largest unstable mode can be found. Besides the initial value solver used for nonlinear simulations, GENE also features an eigenvalue solver for linear simulations which uses test vectors to find the most unstable eigenmodes so that also subdominant and

[1] Short for Gyrokinetic Electromagnetic Numerical Experiment

stable modes can be investigated. Since the perturbed quantities do not saturate, the linear mode cannot be used to find absolute fluxes, though quasilinear estimates can be used, like the so-called mixing length estimate. Stability analysis can also be performed, comparing the growth rates of different modes during different circumstances in order to obtain a qualitative understating of the turbulence. Linear peaking factors and pinch contributions can also be calculated, thus determining whether the mode contributes to an inward or outward pinch.

For the nonlinear simulations, the saturated phase with fully developed turbulence is the interesting part. The radial flux of particles and heat are calculated by multiplying the radial component of the $\mathbf{E}\times\mathbf{B}$ velocity with the perturbed density and pressure, respectively, and averaging in space over a flux surface. It is possible to split up the transport in electrostatic (due to fluctuations in Φ) and electromagnetic (due to fluctuations in $A_{\|}$ and $B_{\|}$) parts. The implementation of the gyrokinetic set of equations in GENE is dimensionless, so all native output is also normalized [36]. The nonlinear simulations are performed until the time series contain enough data in the saturated phase to obtain good statistics. The transport during the linear phase is then discarded in the calculation of the time averaged quantities. Since the values in the resulting time series will be correlated, the uncertainty of quantity x has to be determined through the statistical inefficiency, s, through $\sigma = \sqrt{\mathrm{Var}(x_i)s/N}$, where N is the number of data points. The statistical inefficiency can be estimated from the decay of the auto-correlation function. Nonlinear simulations are costly, requiring on the order of 10^5 CPUh and up for a typical ITG dominated simulation with electromagnetic β effects and non-adiabatic electrons in a flux tube domain. This is only possible on supercomputers. GENE has been shown to scale well on up to 32000 cores. Adding to the cost is the extensive convergence testing needed to make sure that the resolution in the three space and two velocity dimensions is enough to resolve the relevant turbulent features and that the domain is large enough to contain them.

Chapter 5

Summary of papers

In **paper A** impurity transport due to ITG/TE mode turbulence in the core plasma region of JET discharge #67730 was investigated using GENE. Three different models for the magnetic equilibrium were compared. First, a simple circular model, secondly, the $\hat{s} - \alpha$ model which still features a circular cross section but allows for finite Shafranov shift and magnetic shear, thirdly, a realistic experimental MHD equilibrium that also includes effects from triangularity and elongation. The effect from added realism through collisions, sheared toroidal rotation and a 2% carbon background was also investigated. Linearly, it was found that the realistic geometry was destabilizing and shifted the spectrum to higher wavenumbers with lower real frequencies. The nonlinear simulations were consistent with this, showing larger heat and particle transport. The linear and nonlinear impurity peaking factors were lowered for heavy impurities since the inward pure convection, dominated by the curvature pinch, was lowered for the realistic equilibrium. For low charge numbers, the peaking was increased for the shaped equilibrium. This is caused by a larger inward thermopinch, since the real frequency here was lower, according to

$$V_{\nabla T_Z} \sim \left(\omega_r \frac{T_Z}{T_e Z} - \frac{7}{4} \left(\frac{T_Z}{T_e Z} \right)^2 \right) \frac{R}{L_{T_Z}}. \tag{5.1}$$

Further, it was seen that collisions had a pronounced effect on the impurity peaking factors, lowering them for light impurities and increasing them for heavy impurities, both linearly and nonlinearly. Nonlinearly, it was seen that this was due to lower diffusivities for all impurities in the collisional case, thus increasing the peaking factors. The difference

between light and heavy impurities can again be explained through Eq. 5.1 as the spectrum was shifted to higher wavenumbers, associated with higher real frequencies in the collisional case, thus the outward first term will serve to lower the peaking factors again for lighter impurities.

In **paper B** the study of impurity transport due to ITG/TE mode turbulence was expanded to include a self consistent treatment of particle and impurity transport, using linear and nonlinear GENE and a more computationally efficient fluid model. Cyclone Base Case parameters were used which correspond to a ITG dominated H-mode discharge. In the self-consistent treatment, the stationary local profiles corresponding to zero particle flux were found simultaneously for the background electrons and the impurities. This is important since the background density gradient can affect the impurity peaking. The background peaking was found to be sensitive to scans over magnetic shear, collisionality, elongation, temperature ratio and plasma β. Thus the self-consistent treatment is important in these cases and was found to mainly enhance the trends from earlier works that assumed a fixed background. However, for collisionality it was found that the increased peaking found for low collisionality was not accompanied by a corresponding increase in impurity peaking, making reactor relevant low collisionality conditions favourable. The fluid, quasilinear GENE and nonlinear GENE background peaking factors were found to be quantitatively comparable and show the same trends, though the quasilinear simulations showed a somewhat higher sensitivity to the scaled parameter. Comparing the quasilinear background and impurity peaking factors, it was found that the impurity peaking factors were consistently lower than the ones for the background, though showed similar scalings. The effect of main ion isotope was also studied and a slight asymmetry in peaking was found between hydrogen, deuterium and tritium. This may result in a D-T fuel separation in cases of high collisionality or large ion to electron temperature ratios.

In **paper C** the attention was turned towards heat transport in JET plasmas. Two matched pairs of ITER-like wall (ILW) and carbon wall (CW) discharges were modelled using GENE in order to investigate the deterioration in global confinement that has been observed since the change in plasma facing components at JET. The discharges were matched with regards to plasma current, the toroidal magnetic field, applied NBI power, average electron density, safety factor, and triangularity. Linear scans were performed with regards to mismatched dimensionless parameters in the matched pairs. It was found that the relative

change in plasma β, Shafranov shift, R/L_{T_e} and magnetic shear served to destabilize the ILW discharges, while the relative change in collisionality and ion to electron temperature ratio serve to stabilize them. The combined effect of the relative changes in these key plasma parameters caused the ITG mode in ILW discharges to be linearly destabilized compared to the matched CW discharges. This was also observed in nonlinear scans over R/L_{T_i} where it was seen that the normalized heat fluxes were larger in the ILW discharges. The ILW discharges also exhibited larger stiffness. Thus, the core confinement in the ILW discharges was affected by the changes in key plasma parameters compared to the CW discharges. However, these parameters are sensitive to the degradation of the edge pedestal that has been observed in ILW baseline H-mode discharges. Hence, it is expected that the core confinement in the ILW discharges would be improved if the edge pedestals were recovered.

Bibliography

[1] DD Clayton. *Principles of stellar evolution and nucleosynthesis*. McGraw-Hill, 1968.

[2] A Grant. Ignition failed: How america's latest attempt at fusion power fizzled. *Science News*, 183:26–29, 2013.

[3] Merriam-Webster. tokamak, february 2014.

[4] JE Martin. *Physics for Radiation Protection: A Handbook, 2nd Edition, Completely Revised and Enlarged*. Wiley, 2008.

[5] U.S Energy Information Administration. International energy statistics, October 2014.

[6] The secretary-general's advisory group on energy and climate change (EGACC). Energy for a sustainable future - report and recommendations. Technical report, United Nations, 2010.

[7] International Energy Agency. World energy outlook 2013 factsheet. Technical report, International Energy Agency, 2013.

[8] TF Stocker, D Qin, et al. Fifth assessment report of the intergovernmental panel on climate change. Technical report, International Panel on Climate Change, 2013.

[9] PJ Vergragt. How technology could contribute to a sustainable world. *GTI Paper Series*, 28, 2006.

[10] DJC MacKay. *Sustainable Energy - without the hot air*. UIT Cambridge Ltd, 2009.

[11] EG Hertwich, T Gibon, AA Bouman, A Arvesen, S Suh, GA Heath, JD Bergesen, A Ramirez, MI Vega, and L Shi. Integrated life-cycle

assessment of electricity-supply scenarios confirms global environmental benefit of low-carbon technologies. *Proceedings of the National Academy of Sciences*, page 201312753, 2014.

[12] V Giordano, F Gangale, et al. Smart grid projects in europe: lessons learned and current developments. Technical report, European Comission Institute for energy, 2011.

[13] OECD. Uranium 2005 - resources, production and demand. Technical report, OECD, 2006.

[14] GC Unruh. Understanding carbon lock-in. *Energy policy*, 28(March):817–830, 2000.

[15] BM Andreev. Separation of hydrogen isotopes in h2o-h2s system. *Separation Science and Technology*, 36:1949–1989, 2001.

[16] U.S. Geological Survey. Minerals commodity summaries 2014. Technical report, U.S. Geological Survey, 2014.

[17] J Ongena and G Van Oost. Energy for future centuries - prospects for fusion power as a future energy source. *Proceedings of the 11th Carolus Magnus summer school on plasma and fusion energy physics*, 2013.

[18] AM Bradshaw, T Hamacher, and U Fischer. Is nuclear fusion a sustainable energy form? *Fusion Engineering and Design*, 86(9-11):2770–2773, October 2011.

[19] FF Chen. *Introduction to Plasma Physics and Controlled Fusion*. Springer, 1984.

[20] K Ikeda. Iter on the road to fusion energy. *Nuclear Fusion*, 50(1):014002, 2010.

[21] H-S Bosch and GM Hale. Improved formulas for fusion cross-sections and thermal reactivities. *Nuclear Fusion*, 32(4):611, 1992.

[22] J Wesson. *Tokamaks*, volume 149. Oxford University Press, 2011.

[23] RL Miller, MS Chu, JM Greene, YR Lin-Liu, and RE Waltz. Noncircular, finite aspect ratio, local equilibrium model. *Physics of Plasmas (1994-present)*, 5(4):973–978, 1998.

[24] EJ Doyle, WA Houlberg, Y Kamada, V Mukhovatov, TH Osborne, A Polevoi, G Bateman, JW Connor, JG Cordey, T Fujita, et al. Plasma confinement and transport. *Nuclear Fusion*, 47(6):S18, 2007.

[25] RD Hazeltine and JD Meiss. *Plasma confinement*. Courier Corporation, 2003.

[26] H Nordman, J Weiland, and A Jarmén. Simulation of toroidal drift mode turbulence driven by temperature gradients and electron trapping. *Nuclear Fusion*, 30(6):983, 1990.

[27] P Helander and DJ Sigmar. *Collisional transport in magnetized plasmas*, volume 1. Cambridge University Press, 2005.

[28] C Angioni and P Helander. Neoclassical transport of heavy impurities with poloidally asymmetric density distribution in tokamaks. *Plasma Physics and Controlled Fusion*, 56(12):124001, 2014.

[29] JW Conner and HR Wilson. Survey of theories of anomalous transport. *Plasma physics and controlled fusion*, 36(5):719, 1994.

[30] J Weiland. *Stability and Transport in Magnetic Confinement Systems*. Springer, 2012.

[31] ITER Physics Expert Group on Confinement, Transport, ITER Physics Expert Group on Confinement Modelling, Database, and ITER Physics Basis Editors. Chapter 2: Plasma confinement and transport. *Nuclear Fusion*, 39(12):2175, 1999.

[32] AJ Brizard and TS Hahm. Foundations of nonlinear gyrokinetic theory. *Rev. Mod. Phys.*, 79:421–468, Apr 2007.

[33] MJ Pueschel. *Electromagnetic effects in gyrokinetic simulations of plasma turbulence*. PhD thesis, Universität Münster, 2009.

[34] H Doerk. *Gyrokinetic Simulation of Microtearing Turbulence*. PhD thesis, Faculty of Natural Sciences, Ulm University, 2012.

[35] F Merz. *Gyrokinetic simulation of multimode plasma turbulence*. PhD thesis, Universität Münster, 2009.

[36] Gene Development Team. *The Gyrokinetic Plasma Turbulence Code Gene: User Manual*, August 2013.

[37] The GENE team. The GENE Code. `http://genecode.org/`.